High-field magnetization measurements on Er_2Fe_{17} single crystals

M. D. Kuz'min,[1] Y. Skourski,[2] K. P. Skokov,[3] and K.-H. Müller[1]
[1]*Leibniz-Institut für Festkörper- und Werkstofforschung, PF 270116, D-01171 Dresden, Germany*
[2]*Hochfeld-Magnetlabor Dresden (HLD), Forschungszentrum Dresden-Rossendorf (FZD), D-01314 Dresden, Germany*
[3]*Faculty of Physics, Tver State University, 33 Gelabova Street, 170002 Tver, Russia*
(Received 5 February 2007; revised manuscript received 7 April 2007; published 30 May 2007)

If the easy magnetization direction of a 3*d*-4*f* ferrimagnet is perpendicular to a high-symmetry axis, a magnetic field applied in the easy direction may induce a number of first-order transitions, the first (lowest-field) one of which carries the information sufficient for an unambiguous determination of the intersublattice molecular field. This idea has been used to find the molecular field in Er_2Fe_{17}. To this end, magnetization curves have been measured in pulsed magnetic fields of up to 50 T applied along [100] or [001]. In order to obtain a reference value of the molecular field by a conventional method, high-field measurements have also been performed on crystals free to rotate. The molecular fields determined by both techniques are in good agreement with each other as well as with the values deduced from literature data.

DOI: 10.1103/PhysRevB.75.184439 PACS number(s): 75.30.Et, 75.30.Kz

I. INTRODUCTION

The molecular field—a summary quantity expressing the intensity of relevant exchange interactions—is one of two main factors determining the behavior of a rare earth (R) in a solid, the other one being the crystal field (CF). The two cannot be readily disentangled from each other, so in most cases spectroscopic data are unsuitable for deducing the value of the molecular field (or the CF).[1] Important exceptions from this rule are compounds of Gd, which is largely insensitive to CF,[2,3] and certain intermultiplet transitions in light-R-based magnets, e.g., with R=Sm.[4]

For 3*d*-4*f* intermetallics with *heavy* R's, there is also a way to find the intersublattice molecular field, i.e., the field created by the transition metal (T) sublattice and acting on the R sublattice. This quantity can be determined from experiments in high magnetic fields, which force the system to abandon its ferrimagnetic ground state and to evolve gradually toward ferromagnetism.[5,6] Unfortunately, magnetic anisotropy is a hindrance here as well; this time it is not just the anisotropy due to the CF on the R, but also the anisotropy of the T sublattice. Quantitatively tractable data can only be obtained when the anisotropy of at least one of the two sublattices (T or R) is negligible. This requirement is of course satisfied if R=Gd, but such a restriction would limit the scope of the method too severely.

Another more attractive possibility for quantitatively meaningful high-field experiments is to study easy-plane ferrimagnets, i.e., tetra-, hexa-, or trigonal systems where the easy magnetization direction lies in the basal plane. The crucial advantage here is that the 3*d* anisotropy *within* the basal plane is always very small. If the sublattice moments do not leave the basal plane as they rotate under the strong magnetic field, the 3*d* anisotropy can generally be neglected. Therefore, all such systems are amenable to measurements on unclamped samples.[23,25] In such experiments, the mutual orientation of the sublattice moments evolves as if there were no anisotropy at all—the crystal lattice simply follows the rotation of the R moments. If the available magnetic field is sufficient to induce a transition to a noncollinear state, the observed threshold field yields in a ready and unique way a value of the molecular field on the rare earth.

The freely rotating sample technique was originally developed for quasistationary magnetic fields.[23,25] Its implementation in pulsed fields meets with serious difficulties described in some detail in Sec. III. We therefore made it our aim to develop a different method of determining the intersublattice molecular field in easy-plane 3*d*-4*f* ferrimagnets (i.e., in the same systems which are amenable to the conventional freely rotating sample technique). Our intention was to take advantage of the fact that a single anisotropy constant is relevant to this special case.

To test our technique, we naturally chose a well-studied compound, Er_2Fe_{17}. It has a hexagonal Th_2Ni_{17}-type structure (space group D_{6h}^4-$P6_3/mmc$), in which Er occupies two crystallographically nonequivalent sites, 2*b* and 2*d*. The molecular fields seen by Er(2*b*) and Er(2*d*) are strictly speaking distinct. However, the difference appears to be small: thus, the ^{161}Dy Mössbauer spectra of the isomorphous Dy_2Fe_{17} are well represented by a single set of hyperfine parameters even at room temperature.[7] On these grounds, the R atoms in the R_2Fe_{17} compounds with the Th_2Ni_{17}-type structure are often regarded as equivalent. Such an approximation will be adopted in this work, too.

Furthermore, we shall assume that the magnetic moments of the Fe atoms, distributed over four nonequivalent lattice sites, are all parallel to each other, making a single magnetic sublattice. As far as Er_2Fe_{17} is concerned, validity of this approximation is limited to low temperature and ambient pressure. Under a pressure of only 0.2 GPa, the collinear ferrimagnet turns into a helix,[8] just like what happens in Y_2Fe_{17} at a much higher pressure $\sim$1 GPa.[9,10] In a closely related Tm_2Fe_{17} just below room temperature, the helix structure is stable even at ambient pressure.[11]

As regards high-field studies of Er_2Fe_{17}, there was an earlier work on a single crystal[12] as well as $Er_2Fe_{17-x}Al_x$ powder data extrapolated to $x=0$.[14] Nonetheless, we carried out our own high-field magnetization measurements both on fixed and free to rotate single crystals.

The paper is organized as follows. After some preparatory development of theory in Sec. II A the technique is set out in

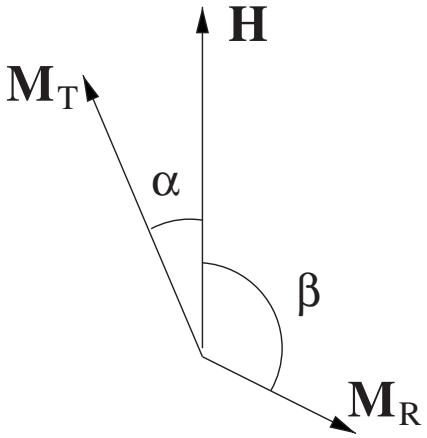

FIG. 1. Mutual orientation of the sublattice magnetizations and applied magnetic field. All three vectors lie in the basal plane of a hexagonal crystal.

Sec. II B. Experimental details are then exposed in Sec. III, followed by results and discussion in Sec. IV.

II. THEORY

A. General

Further to the suppositions stated in the Introduction, we consider a two-sublattice magnet whose sublattice magnetizations, $\boldsymbol{M}_{\mathrm{T}}$ and $\boldsymbol{M}_{\mathrm{R}}$, are assumed spatially homogeneous. Our starting point is the following thermodynamic potential:

$$\Phi(\boldsymbol{M}_{\mathrm{T}},\boldsymbol{M}_{\mathrm{R}},\boldsymbol{H}) = \lambda \boldsymbol{M}_{\mathrm{T}} \cdot \boldsymbol{M}_{\mathrm{R}} - \mu_0 \boldsymbol{H} \cdot (\boldsymbol{M}_{\mathrm{T}} + \boldsymbol{M}_{\mathrm{R}}) + E_a^{\mathrm{T}} + E_a^{\mathrm{R}}. \tag{1}$$

Here, the first term describes the R-T exchange, which favors an antiparallel orientation of the sublattices, $\lambda > 0$. The second term describes the interaction with the applied magnetic field, while the last two terms are anisotropy energies of the T and R sublattices. Our consideration is limited to low temperatures, so we assume $|\boldsymbol{M}_{\mathrm{T}}| = M_{\mathrm{T}} = \mathrm{const}$ and $|\boldsymbol{M}_{\mathrm{R}}| = M_{\mathrm{R}} = \mathrm{const}$. The magnetostatic energy is neglected.

We further assume that the system is a hexagonal easy-plane magnet and that the field $\boldsymbol{H}$ is applied along an easy direction in the basal plane. Then, all three vectors $\boldsymbol{M}_{\mathrm{T}}$, $\boldsymbol{M}_{\mathrm{R}}$, and $\boldsymbol{H}$ will lie in the basal plane. The orientation of $\boldsymbol{M}_{\mathrm{T}}$ and $\boldsymbol{M}_{\mathrm{R}}$ will be described by the angles they make with $\boldsymbol{H}$, α and β, respectively (Fig. 1). The thermodynamic potential then takes the following form:

$$\Phi(\alpha,\beta) = \lambda M_{\mathrm{T}} M_{\mathrm{R}} \cos(\alpha+\beta) - \mu_0 H M_{\mathrm{T}} \cos\alpha - \mu_0 H M_{\mathrm{R}} \cos\beta - |K_{4\mathrm{R}}| \cos 6\beta. \tag{2}$$

We have used the standard expression for the R anisotropy energy appropriate for the hexagonal symmetry[15] and omitted the irrelevant terms which depend on the polar angle θ only, since by the assumption $\theta \equiv \mathrm{const} = \pi/2$. A term in $\cos 6\alpha$ originating from the T sublattice (of order 6 in the weak spin-orbit coupling) has been left out.

The equilibrium orientation of the sublattice vectors is found by minimizing Eq. (2) with respect to α and β. To this end, it is convenient to introduce the following dimensionless variables:

$$h = \frac{\mu_0 H}{\lambda M_{\mathrm{T}}}, \quad \varphi = \frac{\Phi}{\lambda M_{\mathrm{T}}^2}, \quad \kappa = \frac{|K_{4\mathrm{R}}|}{\lambda M_{\mathrm{T}}^2}, \quad m = \frac{M_{\mathrm{R}}}{M_{\mathrm{T}}}. \tag{3}$$

Using these variables, the thermodynamic potential (2) is rewritten as follows:

$$\varphi(\alpha,\beta) = m\cos(\alpha+\beta) - h\cos\alpha - mh\cos\beta - \kappa\cos 6\beta. \tag{4}$$

This expression is readily adaptable for tetragonal easy-plane ferrimagnets through the substitution of $\cos 4\beta$ for $\cos 6\beta$ in the last term.

It is easy to see that Eq. (4) depends essentially on two parameters, κ and m. The latter is just the ratio of the sublattice magnetizations, a readily obtainable quantity. Thus, $m \approx 0.49$ for Er_2Fe_{17}.[16] Without loss of generality, we shall hereafter limit ourselves to a special case of $M_{\mathrm{T}} > M_{\mathrm{R}}$

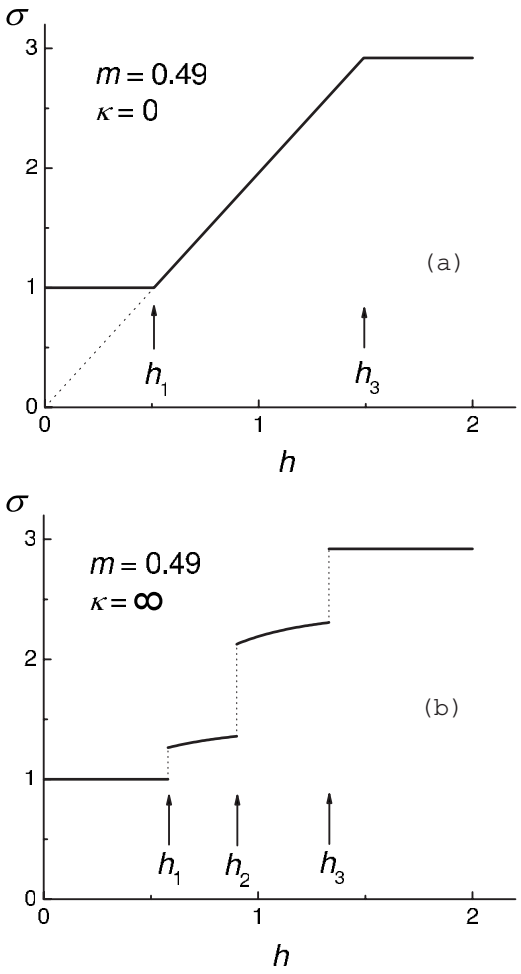

FIG. 2. Reduced magnetization of an easy-plane ferrimagnet versus reduced magnetic field: (a) no in-plane anisotropy [Eq. (6)] and (b) strong six-fold anisotropy, magnetic field parallel to an easy direction [Eq. (7)].

or $0<m<1$, relevant, e.g., to the R_2Fe_{17} compounds. In this case, $\alpha \to 0$ and $\beta \to \pi$ as $h \to 0$ and the magnetization normalized to unity in weak fields is given by

$$\sigma = \frac{\cos\alpha + m\cos\beta}{1-m}. \tag{5}$$

Here, α and β are the equilibrium values of the sublattice orientation angles, obtained by minimizing Eq. (4).

Of primary interest to us is the far from trivial dependence of the magnetization curves $\sigma(h)$ on the unknown anisotropy parameter κ. Explicit expressions for $\sigma(h)$ can only be obtained for the special cases of $\kappa=0$ and $\kappa=\infty$. In the former case, the solution can be found in the literature:[5,6]

$$\sigma(h) = \begin{cases} 1 & \text{if } h < 1-m \\ h/(1-m) & \text{if } 1-m < h < 1+m \\ (1+m)/(1-m) & \text{if } h > 1+m. \end{cases} \tag{6}$$

We also have obtained the following expression for the case of $\kappa=\infty$:[17]

$$\sigma(h) = \begin{cases} 1 & \text{if } h < h_1 \\ [1/(1-m)][(h+m/2)/\sqrt{h^2+mh+m^2} - m/2] & \text{if } h_1 < h < h_2 \\ [1/(1-m)][(h-m/2)/\sqrt{h^2-mh+m^2} + m/2] & \text{if } h_2 < h < h_3 \\ (1+m)/(1-m) & \text{if } h > h_3, \end{cases} \tag{7}$$

where the threshold fields are given by

$$h_1 = \frac{1-m}{1-m/4}, \tag{8}$$

$$h_2 = \sqrt{\frac{1-m^2}{1-m^2/4}}, \tag{9}$$

$$h_3 = \frac{1+m}{1+m/4}. \tag{10}$$

Figure 2 displays both $\sigma(h)$ dependences with $m=0.49$. One can observe that the magnetization curve is continuous in the isotropic case [$\kappa=0$, Fig. 2(a)], but it has three discontinuities when $\kappa=\infty$ [Fig. 2(b)]. They correspond to three first-order transitions, when the R sublattice vector $\boldsymbol{M}_R$ has to jump over a hard direction in the basal plane, on its way from being initially antiparallel to $\boldsymbol{H}$ to becoming eventually parallel to it (see Fig. 3). These transitions in the strongly anisotropic case ($\kappa=\infty$) were earlier analyzed by Franse *et al.*,[18] who used the same approach without succeeding to arrive at the explicit expressions (7)–(10). We also note that in this case the heights of the magnetization jumps at the first (low-field) and the third (high-field) transitions are given by the following simple formulas:

$$\Delta\sigma_1 = \frac{m(1-m/4)}{2-m+m^2/2}, \tag{11}$$

$$\Delta\sigma_3 = \frac{m(1+m)(1+m/4)}{(1-m)(2+m+m^2/2)}. \tag{12}$$

The first one of these expressions (11) is likely to prove useful, since it is the low-field transition that is usually observed experimentally.

In a more realistic case of intermediate κ, $\sigma(h)$ cannot be expressed in explicit form. One may expect intuitively the discontinuities in the $\sigma(h)$ curves to appear at certain finite values of κ, their total number gradually increasing to 3. To perform the calculations numerically, we found it convenient to minimize the potential (4) with respect to the angle α first, and then to eliminate α by means of the resulting expression,

$$\alpha = \arctan\frac{m\sin\beta}{h - m\cos\beta}. \tag{13}$$

Now, the function $\varphi(\alpha(\beta),\beta)$ needs to be minimized with respect to just one variable, β. This was carried out by trial and error, taking for β values between 0 and π in increments

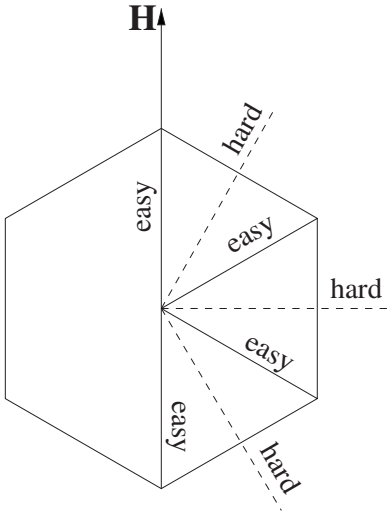

FIG. 3. Easy and hard directions in the basal plane of a hexagonal crystal relevant to the magnetization curve in the strongly anisotropic case [Fig. 2(b)]. As the magnetic field varies, the R sublattice magnetization takes consecutively the four easy directions.

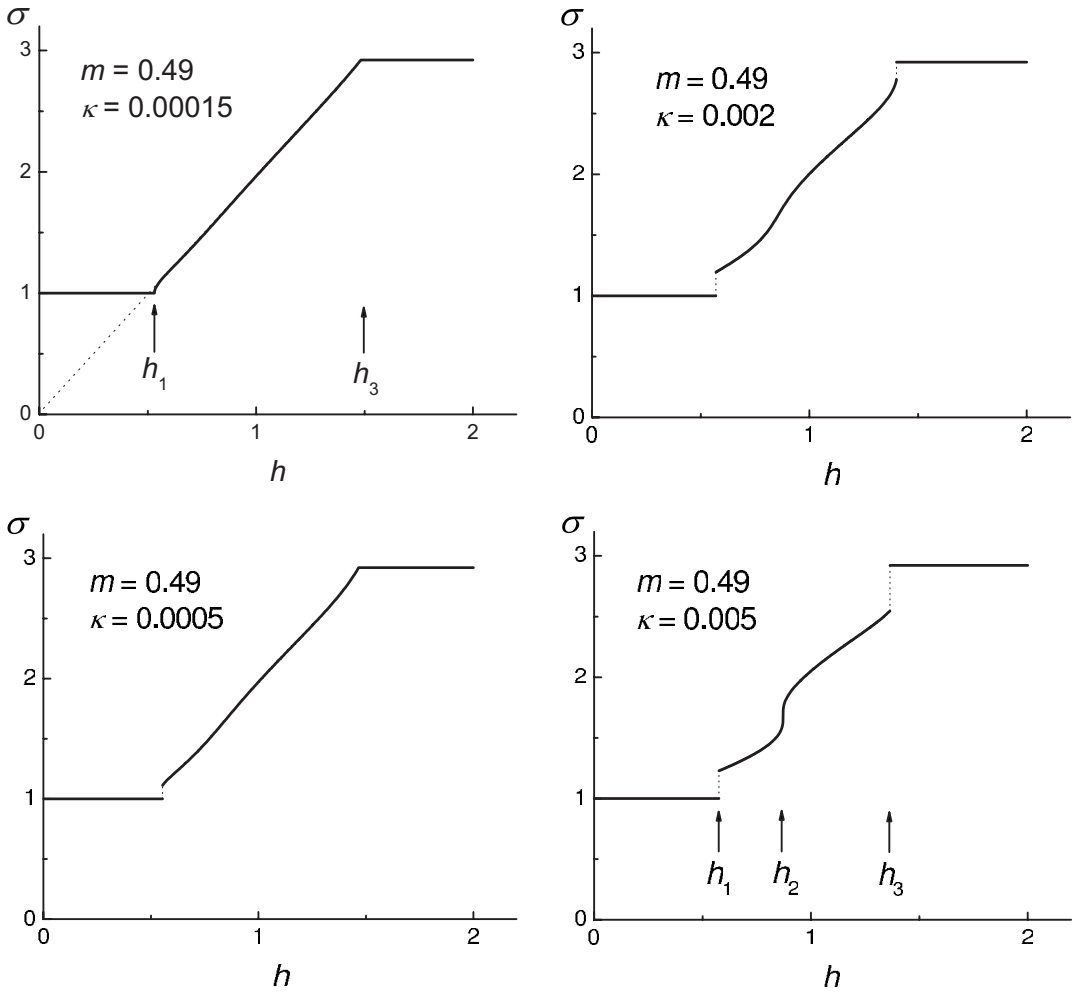

FIG. 4. Magnetization curves calculated numerically for selected intermediate values of the anisotropy parameter κ. The magnetic field is applied in an easy direction.

of 0.001. The obtained equilibrium values of α and β were subsequently put into Eq. (5).

The magnetization curves computed in this way for $m=0.49$ and some representative values of κ are shown in Fig. 4. We observe that for very small κ, the curves are continuous. Then at some stage, as κ grows, the low-field kink becomes a discontinuity. This means that the second-order phase transition turns into a first-order one. Then, at a yet higher κ, the high-field kink undergoes the same transformation. Finally, an S-shaped anomaly develops in the middle part of the magnetization curve.

An exhaustive summary of this information for any given m is afforded by a κ-h phase diagram. Figure 5 is such a diagram for $m=0.49$, as relevant to Er_2Fe_{17}. The solid curves in Fig. 5 are first-order phase transition lines. A magnetization process for a specific system—a growth of the field h at fixed anisotropy κ—is depicted by a vertical line. Where this line crosses a solid curve, a first-order transition (a jump of magnetization) occurs. The solid curves are delimited on the left by critical points, where the former either end (as in the case of an end point C_2) or continue as second-order (dotted) transition lines (as happens at tricritical points C_1 and C_3). The number of jumps in a magnetization curve $\sigma(h)$ of a particular system is thus uniquely determined by its abscissa in Fig. 5, i.e., by its anisotropy parameter κ. In general, the higher the κ, the more jumps take place, up to their total number of 3. There will be no jumps at all if $\kappa<\kappa_{C_1}$.

General expressions for the coordinates of the critical points in a κ-h phase diagram as well as for the second-order (dotted) transition lines are given in the appendixes. Using these formulas, one can sketch diagrams similar to Fig. 5 for any value of m without recourse to large-scale calculations. The shape of these diagrams does not depend on m in the sense that for any m between 0 and 1, the upper line has a descending slope, while the other two lines ascend. The only topological change worthy of mention occurs at $m\approx 0.78$. In the diagrams for smaller m values ($0<m<0.78$) the point C_2 lies to the right of C_3, whereas for larger m ($0.78<m<1$) C_2 lies to the left of C_3.[19] In terms of magnetization curves, this means that when m is fixed at a positive value below 0.78 and κ is gradually increased, the low-field discontinuity at h_1 first appears, followed by the high-field one at h_3, followed by the middle one at h_2. The order of appearance of the jumps at h_2 and h_3 will be reversed if $0.78<m<1$; now at certain κ, the $\sigma(h)$ curves may be discontinuous at h_1 and at h_2, but still continuous at h_3.

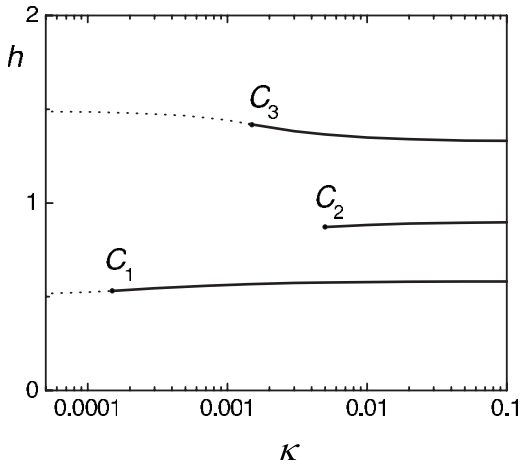

FIG. 5. Phase diagram of a hexagonal easy-plane ferrimagnet. The solid curves are first-order phase transition lines calculated numerically. The second-order (dotted) transition lines and the positions of the critical points were computed using the formulas given in the appendixes with $m=0.49$.

B. Method of determining H_{mol}

By definition (3), the molecular field on the R sublattice is just the ratio of the dimensional and dimensionless magnetic fields, $H_{\mathrm{mol}}=\lambda\mu_0^{-1}M_{\mathrm{T}}=H/h$. Therefore, the problem is solved, $H_{\mathrm{mol}}=H_1/h_1$, if one succeeds to relate the two abscissa scales by (i) observing a field-induced first-order transition at a point H_1 in an experimental curve magnetization versus H (Fig. 6) and (ii) independently finding the position h_1 of the same anomaly in the corresponding theoretical curve $\sigma(h)$.

To determine h_1, we propose to use the measured height of the magnetization jump $\Delta\sigma_1$ (Fig. 6), the magnetization being normalized to unity before the jump. The two quantities, h_1 and $\Delta\sigma_1$, depend on the anisotropy parameter κ in a rather complicated way. However, when the pair of functions $\{\Delta\sigma_1(\kappa), h_1(\kappa)\}$ is regarded as a parametric definition of the dependence $\Delta\sigma_1$ versus h_1 (with $\kappa_{C_1}<\kappa<\infty$), the latter proves practically linear (see Fig. 7).

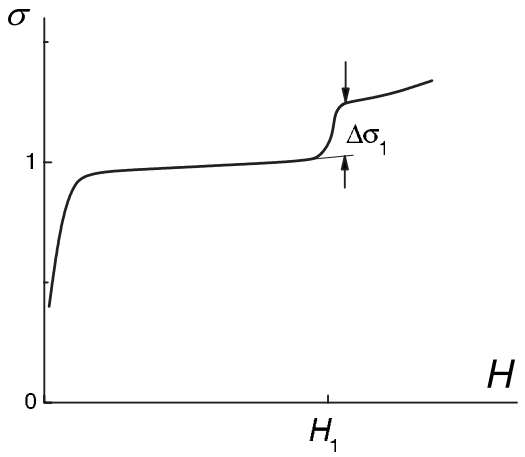

FIG. 6. Schematic normalized magnetization curve with a "jump" corresponding to a first-order phase transition.

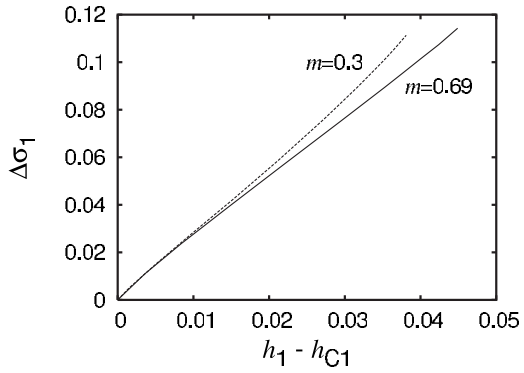

FIG. 7. The height of the first magnetization jump versus the first threshold field, calculated for two representative values of $m \equiv M_{\mathrm{R}}/M_{\mathrm{T}}$. The magnetic field is applied in an easy direction.

Both end points can be readily located. The left-hand extreme is the tricritical point C_1, where the magnetization jump $\Delta\sigma_1$ vanishes and the threshold field takes the critical value h_{C_1} [Eq. (A8)]. At the opposite end of the interval, $\kappa=\infty$, h_1 and $\Delta\sigma_1$ are obtainable from the simple expressions (8) and (11). Interpolating linearly, we get

$$h_1 = h_{C_1}(m) + \Delta\sigma_1\left[\frac{1-m}{1-m/4} - h_{C_1}(m)\right]\frac{2-m+m^2/2}{m(1-m/4)}. \tag{14}$$

Here, $\Delta\sigma_1$ is a quantity to be determined from experiment (Fig. 6) and $h_{C_1}(m)$ is a known function [Eq. (A8)] of the sublattice magnetization ratio m. Having found H_1 and h_1, one gets immediately the molecular field on the R sublattice, $H_{\mathrm{mol}}=H_1/h_1$. Thus, the method does not require any precise knowledge of the anisotropy parameter κ.

III. EXPERIMENTAL DETAILS

The initial components, 99.9% pure Er and 99.998% pure Fe, were mixed in the nominal molar ratio 2:17. The subsequent alloying was carried out in an alundum crucible placed in an induction furnace under argon atmosphere. The melt was cooled down slowly, at a rate of 10 K/min, to facilitate the growth of large single-crystalline grains within the ingot. The ingot was then broken up by ultrasound and large (~200 mg) single-crystalline grains were picked out. The quality of the so prepared single crystals was controlled by means of optical metallography, atomic force microscopy, and x-ray diffraction (back Laue). Specimens without grain boundaries or inclusions of extraneous phases were selected for further processing. First, by grinding off sharp corners, the crystals were roughly shaped into spheres of various sizes. Thereupon, they were run for several hours by a jet of compressed air inside a cylinder lined with fine sandpaper, until they became visually spherical. The stressed surface layers were removed by electropolishing in CrO_3 solution. For magnetization measurements, the crystals were oriented (when required) by back Laue diffraction.

The magnetization measurements were performed at the pulsed-field facility of IFW Dresden. The energy was stored

in a 1 MJ capacitor bank, consisting of four identical 5 mF capacitor modules connected in parallel. The pulsed coil used in the present work had been manufactured by the NHMFL, Tallahassee. Combined with the capacitor bank, it provided a magnetic field of up to 50 T in a 24 mm bore with a rise time of about 8 ms.

The magnetic field was measured by two pickup coils connected in series located symmetrically above and below the sample pickup coils. To avoid possible influence of a magnetized sample on the field value, the field-measuring coils were placed at a reasonable distance from the sample. The signal from the coils, proportional to $\dot{H}$ ($\equiv dH/dt$), was integrated by an analog integrator. The integrator zero was reset just before the start of each pulse and checked again shortly after the end of the pulse to enable correction for drift. The whole field-measuring system was calibrated by measuring the well-known magnetization curve of the MnF_2, where a spin-flop transition takes place at 9.3 T.

The value of the magnetic moment was obtained by measuring the signal induced in a pickup coil surrounding the sample. This signal contained contributions from the changing magnetic moment of the sample $\dot{M}$ ($\equiv dM/dt$) as well as from the varying magnetic field $\dot{H}$. The latter had to be canceled out by the signal from a compensation pickup coil, exposed to the same changing field as the coil with the sample, but connected in the opposite sense. Since perfect compensation of the pickup coils is, in principle, impossible, every measurement of a magnetization curve was followed by a measurement of the decompensation signal, performed in identical conditions but without a sample. This background signal was then subtracted from the initial magnetization curve.

As can be appreciated from the preceding section, the proposed technique is more sensitive to additive uncertainties in M than it is to calibration errors of multiplicative kind. Therefore, correct determination of zero on the magnetization scale—always nontrivial where integration is involved—is essential for the success of the method. To this end, magnetization was also recorded at negative fields (down to about −7 T) during the recoil after the main pulse, then the entire curve was centered around the origin (Fig. 11). The recoil data are not shown in Figs. 9 and 10 to save space.

Two quite different sample pickup coil systems were employed, depending on whether the sample was fixed or free to rotate. The first one, used for measurements on fixed crystals, consisted of a sample coil (sample space ~5 mm in diameter), surrounded by a coaxial compensating coil. The coils were connected via a balancing voltage divider to the input of an analog integrator. The magnetometer (together with the integrator) was calibrated by measuring the well-known magnetization curve of barium ferrite. Further details about this pickup coil system can be found in Ref. 20.

For the measurements on unclamped crystals, the sample size had to be cut down to $R \approx 0.3$ mm in order to reduce the sample reaction time constant, $\tau = (R^2/\mu_0 M\dot{H})^{1/3}$, where M is the mass magnetization and R is the radius of the sample. To prevent the coil filling factor from becoming too low, a new set of smaller pickup coils had to be constructed for the purpose. In this case, the sample and the compensation coils were identical and situated beside each other. The coils were 3 mm long with a 1 mm bore and contained 150 turns.

The mechanism of the delay at the start of rotation of an unclamped ferrimagnet is illustrated in Fig. 8. In a weak magnetic field, the easy axis and both sublattices are perfectly aligned with the field, the sublattice with the larger moment being parallel and the one with the smaller moment antiparallel to the field. The energy of the system is a minimum at $\delta = 0$ [Fig. 8(a)], where δ is the angle between the crystal's easy axis and the direction of the field. As the growing with time magnetic field reaches a critical value H_c, the equilibrium of the collinear alignment becomes unstable, i.e., the energy minimum at $\delta = 0$ turns into a maximum. At the same time, two new minima appear at nonzero δ, situated symmetrically on both sides of the maximum. In the spirit of Landau's theory, the positions of the minima should depend on time as $\delta \propto \pm(H - H_c)^{1/2} = \pm \dot{H}^{1/2} t^{1/2}$, where the zero on the time scale has been chosen to coincide with the moment when the magnetic field reaches the critical value. The solid curve in Fig. 8(b) shows schematically the positive branch of this dependence. The crystal's easy axis cannot keep up with the rapid motion of the energy minima, initially infinitely fast. It cannot even decide which of the two minima to follow. Indeed, the crystal cannot start rotating instantly (and certainly not with an infinite angular velocity) because it experiences no torque at equilibrium, albeit unstable. The crystal will come into rotational motion eventually after the energy maximum has gained sufficient steepness. This process develops in avalanchelike fashion [dashed line in Figs. 8(b) and 8(c)] and very soon the crystal's easy axis catches up with one of the runaway energy minima.[21] So, while in a steady-field magnetization curve of an unclamped crystal the transition point looks like a kink between two straight segments [Fig. 8(c), solid line], the pulsed-field curve (dash) sags due to the inertia of a finite-size sample. This effect is clearly visible in the experimental data (Fig. 11).

The exact duration of this process is hard to evaluate because it is largely determined by factors outside our control: imperfect initial alignment, dry friction, jolts experienced by the sample in a pulsed magnetic field, etc. Roughly, however, one can estimate the catching-up time as 5τ; over this time, the angular velocity increases by three orders of magnitude. The increment of the applied field over the same period of time amounts to $\Delta H = 5\tau\dot{H}$. For a typical crystal ($R \approx 1$ mm) of Er_2Fe_{17} ($M \approx 80$ A m^2/kg) in the pulsed-field installation employed ($\mu_0\dot{H} \approx 1 \times 10^4$ T/s), one gets $\tau = (R^2/\mu_0 M\dot{H})^{1/3} \approx 0.1$ ms and $\mu_0 \Delta H \sim 5$ T. That is, a normal-size crystal does not have enough time to deviate noticeably from the initial orientation $a \| \boldsymbol{H}$ before the applied field reaches the threshold value 37.5 T (see Figs. 10 and 11) and a first-order transition takes place, just as if the crystal were fixed rather than free to rotate. This effect frustrated our early attempts to perform the measurements on relatively large (~2.5 mm in diameter) unclamped crystals; the resulting magnetization curves looked no different to the ones obtained on fixed samples with $a \| \boldsymbol{H}$ (Fig. 10). This brought about the need to substantially reduce the sample size and all the extra difficulties entailed.

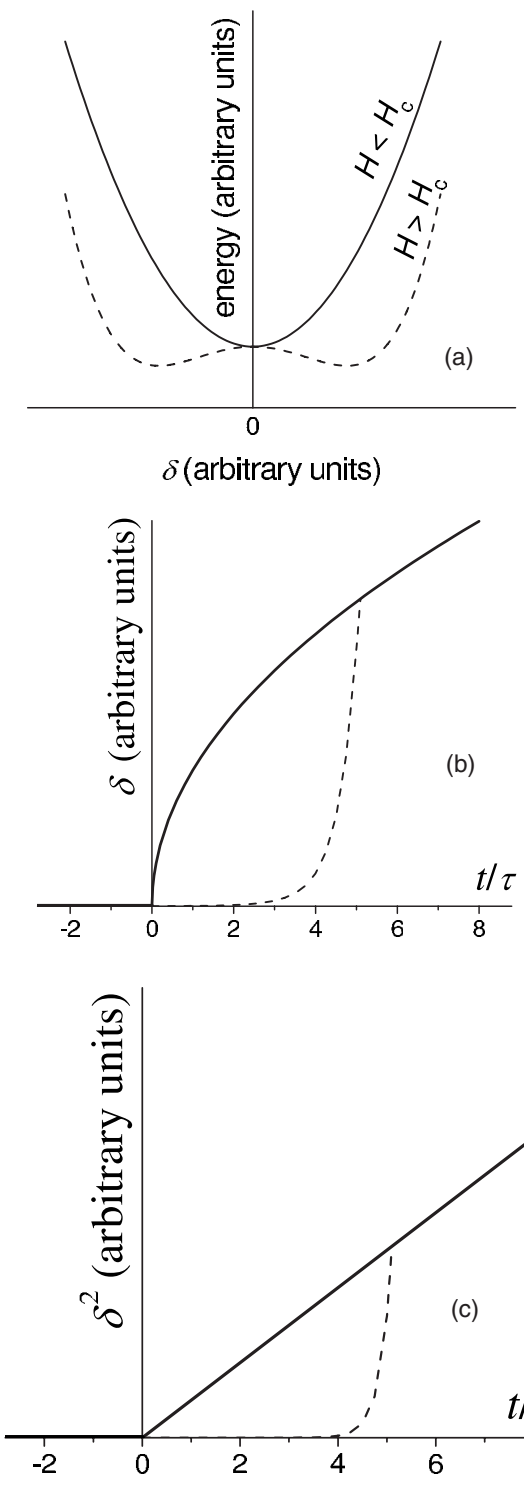

FIG. 8. (a) The energy of a free to rotate ferromagnetic crystal versus the angle δ between its easy axis and the magnetic field. In small fields, the easy direction tends to align itself with the field; the energy is a minimum at $\delta=0$. As at $t=0$ the growing field reaches a critical value H_c, the minimum transforms into a central maximum flanked by two minima. (b) Time dependence of the abscissa of the (right-hand) minimum in the previous graph (solid line) and the actual orientation angle of the crystal's easy axis (dash). (c) The respective contributions to the magnetization projection on the direction of the applied magnetic field, $\propto\delta^2$.

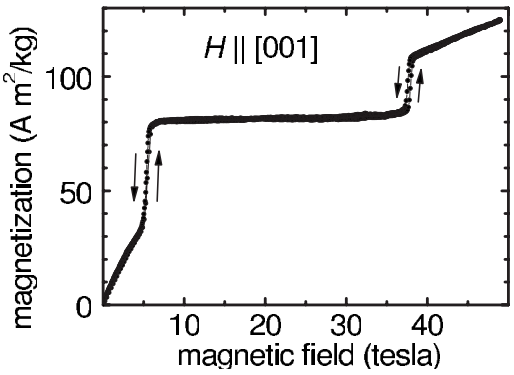

FIG. 9. Magnetization curve of Er_2Fe_{17} measured along [001].

IV. RESULTS AND DISCUSSION

Figure 9 presents a magnetization curve of Er_2Fe_{17} measured along the hard axis c [001]. At about 5 T, one can clearly see a first-order field-induced spin-reorientation transition (SRT) earlier observed by several authors,[22] in particular, by Sinnema.[23] (It will be recalled that an SRT does not affect the mutual orientation of the sublattices, antiparallel in this case; only their orientation in relation to the crystallographic axes changes.) A second first-order transition takes place at about 38 T (the field in Sinnema's experiments[23] went up to 35 T). This transition cannot be classified as an SRT because departure from the antiparallel orientation of the sublattices is essential here. Theoretically, it was predicted over a decade ago by Zhao *et al.*[24] The predicted threshold field, 36.7 T, agrees surprisingly well with experiment, especially if the latter is corrected for effects of demagnetization. For our purpose, however, this threshold field is a less valuable source of information, since it depends on several crystal-field parameters.

Our main objective is to analyze easy-axis magnetization curves, for which a quantitative model has been developed in Sec. II. Such a curve, measured in $\boldsymbol{H}\|a$ or [100], is displayed in Fig. 10. Two first-order transitions are evident. The higher-field one is centered around 44 T and features an ~2-T-wide hysteresis loop. Of primary interest to us, however, is the lower-field transition. It is situated at $\mu_0 H_1=37.5$ T, the hysteresis being rather narrow, ~0.5 T. For the relative height

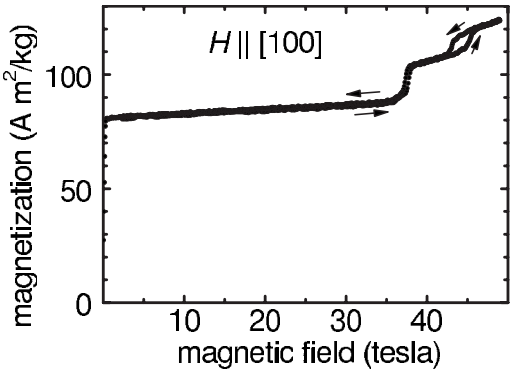

FIG. 10. Magnetization curve of Er_2Fe_{17} measured along [100].

TABLE I. Molecular field on Er determined by means of Eq. (14) using experimental data from various sources.

$\mu_0 H_1$ (T)	$\Delta\sigma_1$	h_1	$\mu_0 H_{mol}$ (T)
37.5[a]	0.18[a]	0.565	66.4
35.7[b]	0.18[b]	0.565	63.2
33.5[c]		0.51	65.7
			66.7[d]

[a]This work.
[b]Reference 12.
[c]Freely rotating crystal, $h_1=1-m$, this work.
[d]$Er_2Fe_{17-x}Al_x$ powder data extrapolated to $x=0$, Ref. 14.

of the magnetization jump (see Fig. 6), we find $\Delta\sigma_1 \approx 0.18$. Equations (A8) and (14) yield for Er_2Fe_{17} ($m=0.49$) $h_{C_1}=0.531$ and $h_1=0.565$. Hence, the molecular field on the Er sublattice is $\mu_0 H_{mol}=\mu_0 H_1/h_1=66.4$ T. This and similar results are collected in Table I for comparison.

For verification, H_{mol} was also determined using the traditional technique, from a magnetization curve measured on a small single-crystalline sphere free to rotate (Fig. 11). The measurements were performed on the more sensitive, purpose-made magnetometer (Sec. III), without calibration. For reasons explained in the previous section, the magnetization curve is distorted around the transition point. The threshold field, $\mu_0 H_1=33.5$ T, was determined by extrapolation of the linear portions of the curve below and above the transition. Hence, we got the molecular field on Er, $\mu_0 H_{mol}=\mu_0 H_1/(1-m)=65.7$ T, as listed in Table I.

For a more complete comparison, we applied our technique to an earlier published magnetization curve along [100].[12] We also included in Table I the value of H_{mol} obtained in Ref. 14 by extrapolation to $x=0$ of $Er_2Fe_{17-x}Al_x$ powder data (cited in Ref. 14 is the so-called exchange field on Er, $\mu_0 H_{ex}=3\mu_0 H_{mol}=200$ T).

Comparing the values in the last column of Table I, it is worth noting that these should be in all rigor rounded to two digits. While on the whole the values appear consistent, the two of them obtained in this work differ by as little as 1%. We thus may conclude that our technique has passed the test.

We now turn to the higher-field transition in Fig. 10, situated at about 44 T. Earlier, a similar transition was observed at 42 T by Verhoef *et al.*[12] As regards the nature of this anomaly, it clearly cannot be identified with the transition at h_2 shown in Fig. 2(b) or in the lower right panel of Fig. 4. Such a transition could only take place at a higher field, about 56 T (because $h_2/h_1 \approx 1.5$). The most likely explanation is that proposed by Verhoef *et al.*[12] and later adopted by Zhao *et al.*[24] and García-Landa *et al.*[13] According to this scenario, the sublattice moments leave the basal plane and go over into the plane *ac*, or (010). A quantitative description of such a transition would necessitate a generalization of the model set out in Sec. II by way of introducing several additional free parameters, which is outside the scope of this work. (We would like to remind at this point that our main goal is a *unique* deduction of the molecular field from the observation of the first, lower-field transition. The presence of another transition at a higher field does not interfere with our reasoning.) Continuing with the higher-field transition, we note its reentrant character: the sublattices leave the basal plane at a certain value of applied field but later, at a yet higher field, they suddenly return to the basal plane. The width of the interval between the two threshold fields depends strongly on the adopted parameters, e.g., from 49.5 to 63.0 T in Ref. 24 and from 53.5 to 58.5 T in Ref. 13, centered always around 56 T. It means that the parameter set of Ref. 13 is nearly three times closer than that of Ref. 24 to the threshold beyond which the sublattices do not leave the basal plane at all (i.e., everything proceeds as described in Sec. II). The latter scenario cannot therefore be ruled out, since it lies near the sets of Refs. 13 and 24 in parameter space.

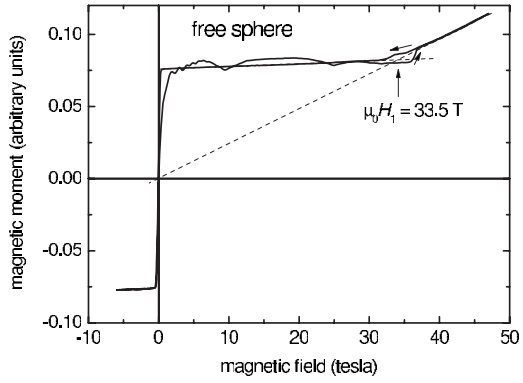

FIG. 11. Magnetization curve measured on an unclamped single crystal of Er_2Fe_{17}.

Because of the discrepancies in the calculations of the higher-field transition, it would be of interest to measure the magnetization along the *a* axis up to a higher field (100 T) in order to observe all possible transitions. This would enable one to clarify the complex behavior of Er_2Fe_{17}, characterized by the presence of several competing contributions to the anisotropy energy. On account of this complexity, Er_2Fe_{17} was perhaps after all not the best choice for our case study. The advantages of our method will become more apparent when applied to R_2Fe_{17} where the Stevens factor α_J is negative (i.e., R=Tb,Dy,Ho) so that the second-order crystal field favors the easy-plane structure instead of opposing it.

In summary, magnetization curves of Er_2Fe_{17} have been measured at $T \approx 10$ K in a long-pulsed field up to 50 T, applied either to a fixed crystal or to a crystal free to rotate. In a field applied in the hard direction [001], a previously known first-order transition has been observed at 5 T, and a further first-order transition has been observed at about 38 T. In a field applied along the easy axis [100], a first-order transition at 37.5 T has been observed, followed by another first-order transition at about 44 T. The threshold field of the former (37.5 T) has been used to deduce—using the proposed technique—the molecular field on Er. This has been found to agree well with the value obtained by a more direct (but experimentally more demanding) method, from measurements on an unclamped sample. Also, earlier published data, processed using the proposed technique, have yielded consistent molecular field values. In our view, the proposed technique has the potential of becoming a standard method of experimental determination of intersublattice molecular field in ferrimagnets.

ACKNOWLEDGMENTS

The authors are grateful to F. R. de Boer and A. V. Andreev for their helpful critique of the paper. Work at the University of Tver (sample preparation) was financially supported by the Russian Foundation for Basic Research, Grant No. 05-02-17197. Theoretical work at IFW Dresden received financial support from Deutsche Forschungsgemeinschaft through Project No. RI 932/4-1.

APPENDIX A: TRICRITICAL POINTS AND SECOND-ORDER TRANSITION LINES IN THE PHASE DIAGRAM

Let us first deal with the lower second-order (dotted) line ending at the tricritical point C_1 (Fig. 5). Two simultaneous equations obtained by minimizing the thermodynamic potential $\varphi(\alpha,\beta)$ [Eq. (4)],

$$-m\sin(\alpha+\beta)+h\sin\alpha=0, \tag{A1}$$

$$-m\sin(\alpha+\beta)+mh\sin\beta+6\kappa\sin 6\beta=0, \tag{A2}$$

are to be solved under an additional condition that the system deviates little from the ferrimagnetic ground state. That is, the angle α must be infinitesimally small, and β must be presentable as $\beta=\pi-\eta$, where η is an infinitesimal quantity. It is convenient to rewrite Eq. (A1) as Eq. (13) and to use it to eliminate α from Eq. (A2). The latter is then presented as an expansion in odd powers of the small parameter η:

$$a\eta+b\eta^3+\cdots=0, \tag{A3}$$

where

$$a=mh\left(\frac{1}{m+h}-1\right)+36\kappa, \tag{A4}$$

$$b=-\frac{1}{6}a+\frac{m^2h^2}{2(m+h)^3}-210\kappa. \tag{A5}$$

According to Landau, in order for a second-order phase transition to take place, it is necessary that $a=0$ and $b>0$. Equating Eq. (A4) to zero yields immediately

$$\kappa=\frac{mh}{36}\left(1-\frac{1}{m+h}\right), \tag{A6}$$

which can be also presented as $h(\kappa)$:

$$h=\frac{1}{2}\left[1-m+\frac{36\kappa}{m}+\sqrt{\left(1-m+\frac{36\kappa}{m}\right)^2+144\kappa}\right]. \tag{A7}$$

This expression, with $m=0.49$, describes the lower dotted curve in the phase diagram (Fig. 5).

At a tricritical point, where a second-order transition turns into a first-order one, both Landau's coefficients must vanish: $a=0$, $b=0$. Equation (A5) then yields

$$\kappa=\frac{1}{420}\frac{m^2h^2}{(h+m)^3}$$

which has to be solved simultaneously with Eq. (A6). Eliminating κ, one arrives at an equation cubic in h. It has three real solutions, but only one of them is positive. This positive solution,

$$h_{C_1}=\frac{1}{3}-m+\frac{2}{3}\sqrt{1+\frac{9}{35}m}\times\cos\left[\frac{1}{3}\arccos\frac{1+\frac{27}{70}m-\frac{81}{70}m^2}{\left(1+\frac{9}{35}m\right)^{3/2}}\right], \tag{A8}$$

is the ordinate of the tricritical point C_1. The abscissa is then obtainable from Eq. (A6).

Explicit expressions for the upper dotted line in the phase diagram (Fig. 5) and for the coordinates of the tricritical point C_3 are obtained by merely substituting $-m$ for m in Eqs. (A6)–(A8).

On the left-hand side of the phase diagram (as $\kappa\to 0$) the two dotted curves level off at $h_{1,2}=1\pm m$, whereas on the right ($\kappa\to\infty$) the three solid curves tend to the limits given by Eqs. (8)–(10). Unfortunately, the solid curves themselves cannot be calculated but numerically. However, the position of the remaining critical point C_2 can be estimated rather accurately using simple formulas (B1) and (B4) derived in Appendix B.

APPENDIX B: POSITION OF THE CRITICAL POINT C_2

The key assumption here is that the angle β is very close to $\pi/2$. The ordinate of the point C_2 is obtained by simply putting $\beta=\pi/2$ into the simultaneous equations (A1) and (A2). It follows immediately that $\sin\alpha=m$ and

$$h_{C_2}=\cos\alpha=\sqrt{1-m^2}. \tag{B1}$$

To find the abscissa, one has to allow for a small deviation of β from $\pi/2$: $\beta=\pi/2+\eta$. Proceeding as in Appendix A, i.e., using Eq. (13) to eliminate α from Eq. (A2) and expanding the latter in powers of η, we get

$$mh\left(1-\frac{1}{\sqrt{m^2+h^2}}\right)+\left[\frac{m^2h^2}{(m^2+h^2)^{3/2}}-36\kappa\right]\eta+\cdots=0. \tag{B2}$$

The left-hand side of this equation depends on η both explicitly and through h, which is a function of η. The full derivative with respect with respect to η is of course identically nil:

$$\frac{d}{d\eta}(\text{left-hand side})\equiv\frac{\partial}{\partial\eta}(\text{lhs})+\frac{dh}{d\eta}\frac{\partial}{\partial h}(\text{lhs})\equiv 0. \tag{B3}$$

At the critical point C_2, where $dh/d\eta$ vanishes, the *partial* derivative of the left-hand side of Eq. (B2) with respect to η must vanish, too. Equating the square bracket of Eq. (B2) to zero and substituting $1-m^2$ for h^2 [by virtue of Eq. (B1)], we finally get

$$\kappa_{C_2}=\frac{1}{36}m^2(1-m^2). \tag{B4}$$

[1] M. Loewenhaupt and I. Sosnowska, J. Appl. Phys. **70**, 5967 (1991).
[2] M. Loewenhaupt, P. Tils, K. H. J. Buschow, and R. S. Eccleston, J. Magn. Magn. Mater. **138**, 52 (1994).
[3] M. Loewenhaupt, P. Tils, K. H. J. Buschow, and R. S. Eccleston, J. Magn. Magn. Mater. **152**, 10 (1996).
[4] M. D. Kuz'min, L. Steinbeck, and M. Richter, Phys. Rev. B **65**, 064409 (2002).
[5] S. V. Tyablikov, Fiz. Met. Metalloved. **3**, 3 (1956).
[6] A. E. Clark and E. Callen, J. Appl. Phys. **39**, 5972 (1968).
[7] P. C. M. Gubbens and K. H. J. Buschow, J. Phys. F: Met. Phys. **12**, 2715 (1982).
[8] A. S. Andreenko, S. A. Nikitin, and Y. I. Spichkin, Sov. Phys. Solid State **34**, 972 (1992).
[9] S. A. Nikitin, A. M. Tishin, M. D. Kuz'min, and Y. I. Spichkin, Phys. Lett. A **153**, 155 (1991).
[10] O. Prokhnenko, J. Kamarád, K. Prokeš, Z. Arnold, and A. V. Andreev, Phys. Rev. Lett. **94**, 107201 (2005).
[11] D. Givord and R. Lemaire, in *Proceedings of International Conference on Magnetism, 1973* (Nauka, Moscow, 1974), Vol. III, p. 492.
[12] R. Verhoef, F. R. de Boer, S. Sinnema, J. J. M. Franse, F. Tomiyama, M. Ono, M. Date, and A. Yamagishi, Physica B **177**, 223 (1992).
[13] B. García-Landa, P. A. Algarabel, M. R. Ibarra, F. E. Kayzel, and J. J. M. Franse, Phys. Rev. B **55**, 8313 (1997).
[14] J. P. Liu, F. R. de Boer, P. F. de Châtel, R. Coehoorn, and K. H. J. Buschow, J. Magn. Magn. Mater. **132**, 159 (1994).
[15] S. Chikazumi, *Physics of Ferromagnetism* (Clarendon, Oxford, 1997).
[16] Proceeding from the magnetization below the transition, $M=82$ A m^2/kg, or 18.8 μ_B/f.u., and taking for M_{Er} the free-ion value, 18 μ_B/f.u., we get $M_{\mathrm{Fe}}=36.8$ μ_B/f.u. and $m=M_{\mathrm{Er}}/M_{\mathrm{Fe}}\approx 0.49$.
[17] In this case, there are four distinct phases characterized by the orientation of the R sublattice β. To arrive at Eq. (7), one should put $\beta=0$, $\pi/3$, $2\pi/3$, or π into Eq. (4), omitting the last term thereof, minimize it with respect to α, then use Eq. (5). The threshold fields of the first-order transitions (8)–(10) are obtained by equating the equilibrium energies of the appropriate phases. These should be distinguished from the so-called lability fields, limiting the extension of the hysteresis loops. Since no significant hysteresis is observed experimentally in these transitions, the lability fields are left out of consideration.
[18] J. J. M. Franse, R. J. Radwański, and S. Sinnema, J. Phys. (Paris), Colloq. **49**, C8-505 (1988).
[19] The crossover is to be expected at some point between $m=0$ and $m=1$. Indeed, for m small, $\kappa_{C_3}\approx\frac{1}{420}m^2\ll\frac{1}{36}m^2\approx\kappa_{C_2}$. At the other end of the interval, as $m\to 1$, κ_{C_2} becomes infinitesimally small again, while κ_{C_3} tends to a finite limit, ≈ 0.02.
[20] D. Eckert, R. Grössinger, M. Doerr, F. Fischer, A. Handstein, D. Hinz, H. Siegel, P. Verges, and K.-H. Müller, Physica B **294-295**, 705 (2001).
[21] The solution of the equation of motion, $\ddot{\delta}=\tau^{-3}t\delta$, can be expressed in terms of the modified Bessel function of order one-third: $\delta=\mathrm{const}\sqrt{t/\tau}I_{1/3}(2t^{3/2}/3\tau^{3/2})$.
[22] This kind of phase transition is sometimes inaptly called first-order magnetization process.
[23] S. Sinnema, Ph.D. thesis, University of Amsterdam, 1988.
[24] T. S. Zhao, T. W. Lee, K. S. Pang, and J. I. Lee, J. Magn. Magn. Mater. **140-144**, 1009 (1995).
[25] R. Verhoef, R. J. Radwański, and J. J. M. Franse, J. Magn. Magn. Mater. **89**, 176 (1990).